Supporting Information for "Twinning Superlattice Formation in GaAs Nanowires"

Tim Burgess, Steffen Breuer, Philippe Caroff, Jennifer Wong-Leung, Qiang Michael Gao, Hark Hoe Tan, and Chennupati Jagadish

S1 Nanowire areal density

Figure S1 presents lower magnification SEM images of the nanowire growths discussed in figure 3. Measured areal densities are indicated in the figure caption.

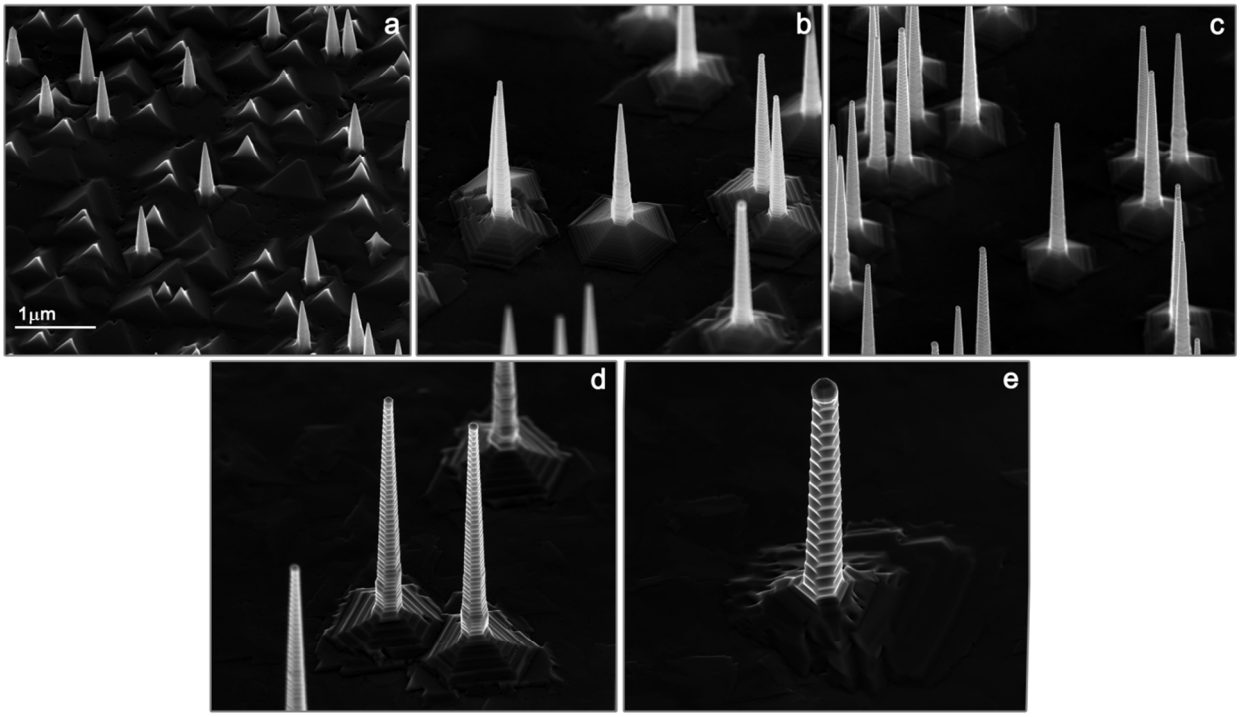

Figure S1. Nanowire areal density; SEM images for each of the Au colloid diameters, (a) 10 nm - 1.73 nanowires/μm^2, (b) 30 nm - 0.15 nanowires/μm^2, (c) 50 nm - 0.21 nanowires/μm^2, (d) 100 nm - 0.09 nanowires/μm^2, and (e) 250 nm - 0.032 nanowires/μm^2. All images were taken at a constant magnification with the sample substrate tilted 45° relative to the incident electron beam.

*Corresponding author: tim.burgess@anu.edu.au

S2 Gibbs Thompson effect

Figure S2 demonstrates the significance of the Gibbs Thompson effect in reducing the effective supersaturation of smaller diameter nanowires under the described growth conditions. Seen inset are magnified views of four Au nanoparticles increasing in size from left to right. The smallest of these (S2(b)) was below the diameter threshold for growth and has not seeded a nanostructure instead forming a pit as described. The other three (S2(c-e)) are seen to have seeded nanostructures which increase in height with increasing Au particle size.

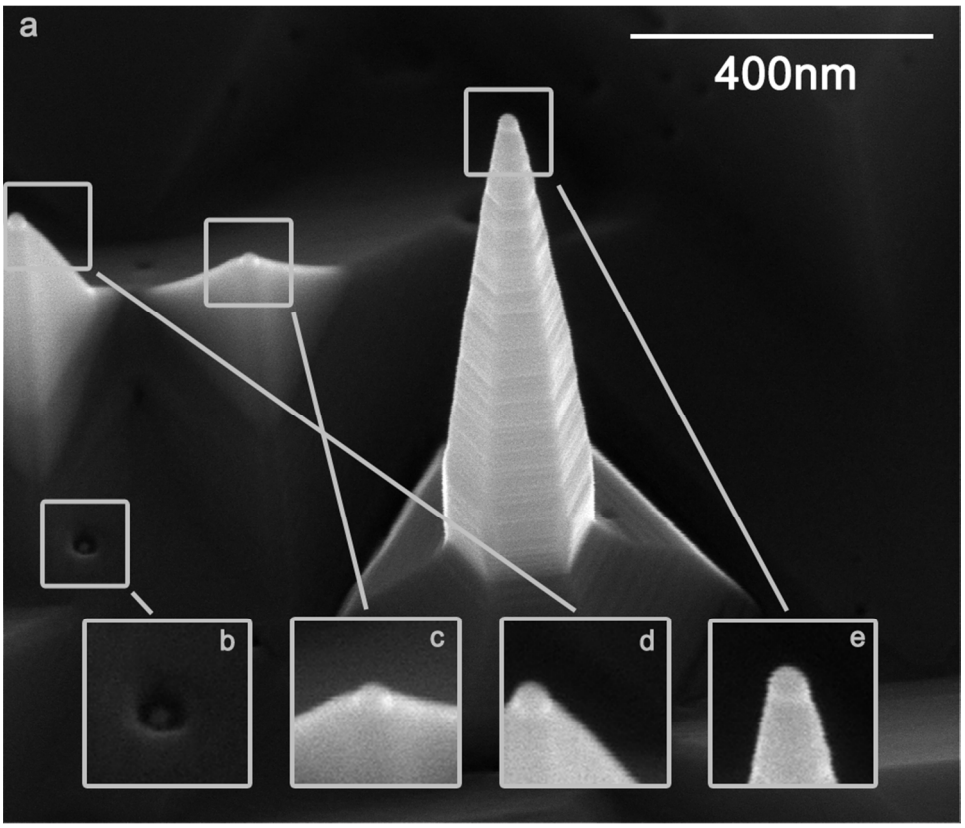

Figure S2. Gibbs Thompson effect; SEM image showing several Au particle sizes, (b) pit formed by Au particle below the threshold for growth, (c-e) increasing nanowire length with increasing Au seed particle diameter. The sample substrate was tilted 45° relative to the incident electron beam

S3 High resolution transmission electron microscopy

Figure S3 presents selected high resolution transmission electron microscopy of nanowires seeded by each colloid size investigated. The randomly twinned ZB region formed on growth termination is clear in S3(c). Note that the convex intersection of facets is below the twin boundary in S3(d) while the concave intersection is at twin boundary in S3(e).

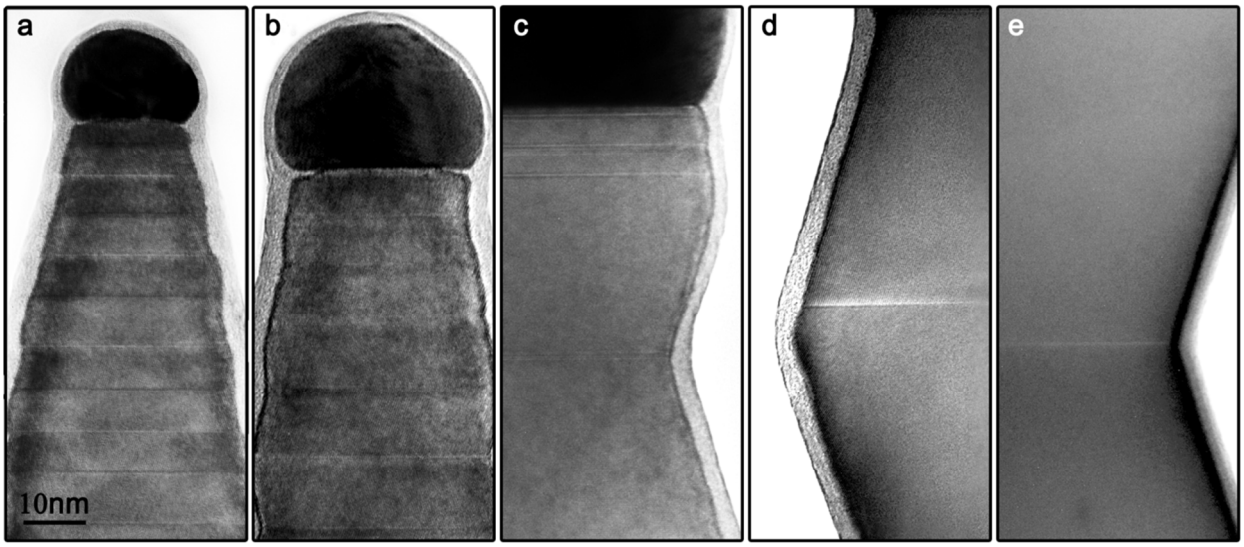

Figure S3. Representative ⟨110⟩ zone axis HRTEM from each of the Au colloid treatments, (a) 10 nm, (b) 30 nm, (c) 50 nm, (d) 100 nm and (e) 250 nm.

S4 Orientation of {111}B facets following overgrowth

Figure S4 presents the distribution of sidewall orientations as altered from the expected {111}B orientation by overgrowth. The measurements are expressed as the angular difference between the orientation of the sidewall projection at the twin boundary closest to the growth front and a perfect {111}B orientation. (shown schematically in figure S3(a)) That the facet orientation remains approximately perpendicular to the ⟨110⟩ zone axis is observed for the case

of larger diameter nanowires from figure S3(b). Indicated are two convex intersection of facets where the small edge arising from this intersection is clearly shifted down (opposite the growth direction) relative to the longer adjacent edge arising from the concave intersection facets. Despite overgrowth, both facet normals appear to remain perpendicular to ⟨110⟩. Comparing the distribution of orientations for each of the representative nanowire diameters it is apparent that the nanowire density (see section S1) has affected final orientation with those nanowires grown with higher areal densities (33nm & 48nm samples) exhibiting lower angular variations. Some clustering around significant orientations is also noted.

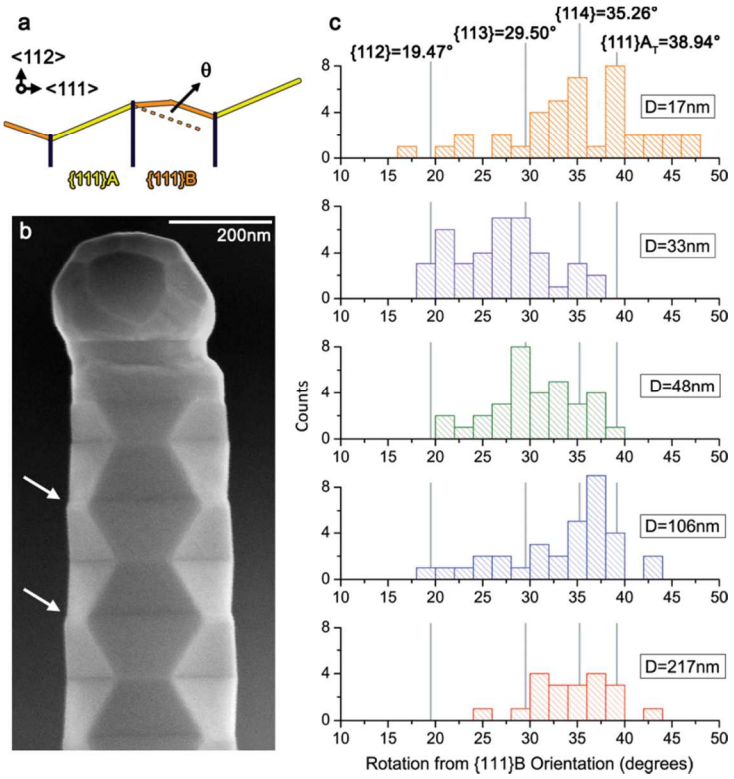

Figure S4. Orientation of {111}B facets following overgrowth: (a) schematic defining the angle of rotation measured; (b) SEM image demonstrating that overgrowth at the convex intersection of facets retains an orientation approximately parallel to the ⟨110⟩ direction; (c) distribution of the orientation of overgrowth as defined by (a) and measured for single nanowires representative of each Au particle size investigated. The $\{111\}A_T$ plane belongs to the crystal twin.

S5 Geometry and physical parameters

Figure S5 illustrates schematically the various geometrical and physical parameters used in this work.

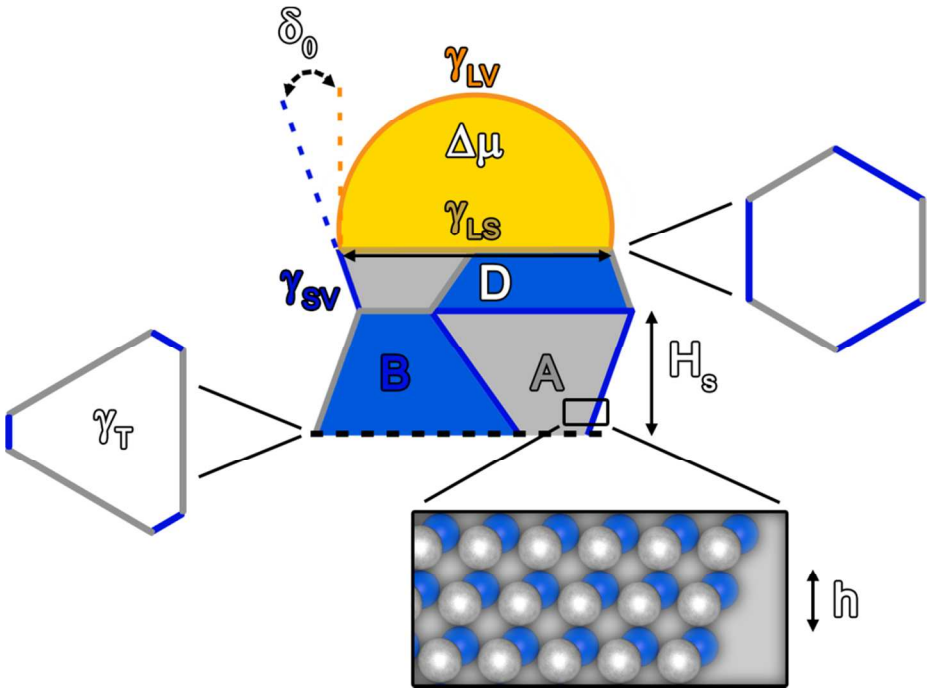

Figure S5. Geometry and physical parameters; γ_T, γ_{SL}, γ_{SV} and γ_{LV} are the surface energies per unit area of a twin plane, the solid liquid, solid vapor and liquid vapor interfaces respectively, $\Delta\mu$ the supersaturation in the Au seed as defined by the difference in chemical potential between III-V pairs in solution relative to those in the solid, δ_0 the angle of the droplet with respect to a {111}B facet at a hexagonal cross section, h the planar bilayer spacing in the $\langle 111 \rangle$ direction, D the nanowire diameter

S6 Derivation of H_c used in this work

In their 2011 work, Algra *et al.* [19] express H_c in the following form;

$$H_c = ADh \qquad \ldots(S1)$$

$$A = \frac{\tilde{A}}{1 + \frac{\tilde{A}gh}{\Delta}} \quad \ldots(S2)$$

$$\tilde{A} = \frac{b}{h^2} \frac{\gamma_T}{\gamma_{LV} \sin\delta_0} \left(\frac{\Gamma}{\Delta\mu}\right) \quad \ldots(S3)$$

Where g is a geometrical constant, which equals 4.46. Examining equation S2, it may be readily appreciated that as Δ increases $\tilde{A}$ becomes a better approximation for the variable A. In our results we have discussed how the twin plane surface energy γ_T of GaAs is relatively large and it is therefore not unreasonable to expect the value of the barrier to twin formation Δ to also be relatively large. Testing this deduction we have fitted equation (2) to our data using both the above definition of H_c (equations S2-4) and the assumption $A = \tilde{A}$ finding a difference of only 0.8% in the value of $\Delta\mu$ and 1° in δ_0. As this simplification thus makes negligible difference to our analysis we chose the form of H_c presented in equation (1) in order to improve clarity for the reader.

S7 Numerical illustration of modeled segment length behavior

Figure S6 presents the expected influence of various physical parameters on twin plane spacing as described by equation (2). The values and the ranges they describe were chosen to be both close to those calculated and/or used in the current work but also illustrative of the general behavior of equation (2). A strong influence of both supersaturation and twin plane surface energy are observed as discussed in our main body of results. A similarly strong influence of solid liquid interfacial energy is also apparent reinforcing the importance of any possible liquid ordering as discussed by Algra *et al.* [2] Finally we note that although the equilibrium contact

angle is also critical it is likely to remain a fitted parameter as measurement and/or calculation has proven difficult.[3]

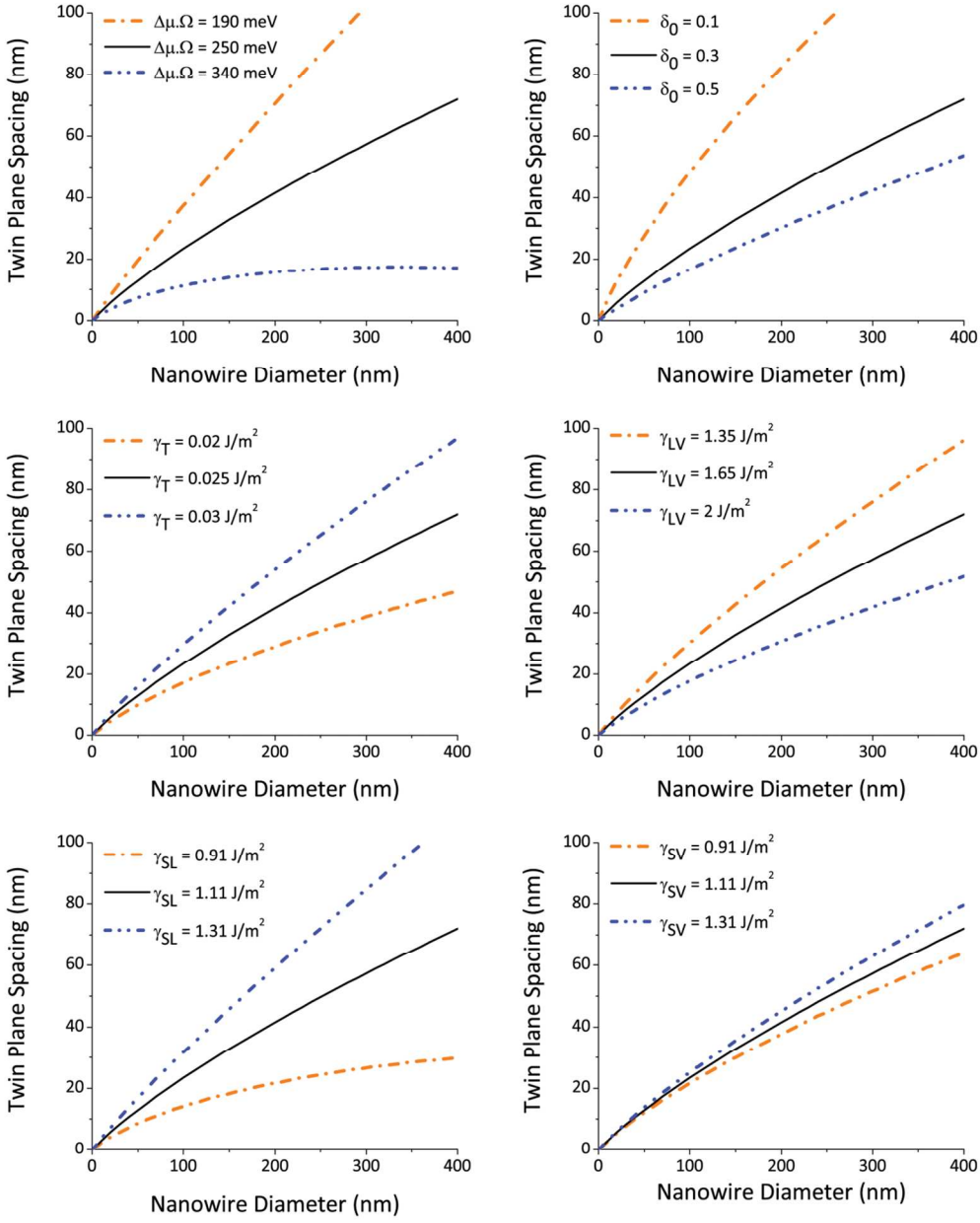

Figure S6 Modeled influence of physical parameters on the relationship between twin spacing and nanowire diameter. The parameters used for the common curve shown in black are the mid range values in each case; $\Delta\mu.\Omega = 250meV$, $\delta_0 = 17.2°$, $\gamma_{LV} = 1.65\,\mathrm{J/m^2}$, $\gamma_T = 0.025\,\mathrm{J/m^2}$, $\gamma_{SL} = 1.11\,\mathrm{J/m^2}$, $\gamma_{SV} = 1.11\,\mathrm{J/m^2}$.

S8 Relationship between supersaturation and growth rate

The relationship between growth rate and supersaturation was approximated for a nucleation limited growth regime by Algra *et al.* [1];

$$v \cong a \cdot \exp\left(-c_1 \frac{\Gamma^2}{\Delta\mu}\right) \quad \ldots(S4)$$

where a and c_1 are constants for given growth conditions. Due to the exponential relationship, small increases in supersaturation $\Delta\mu$ will result in relatively large increases in growth velocity v for physically relevant values of the other parameters.

S9 Comparison of linear fit and model

Although the relationship between diameter and twin spacing found for GaAs may be well represented by a simple linear fit to give an already excellent coefficient of determination (R^2) value of 0.995 we note that the fit of our equation (2) gives an even better value of 0.998. As the linear fit in this case was constrained to pass through the origin and thus has one less fitting parameter we further compared models using the Akaike information criterion where a lower score confirmed equation (2) as the preferred model.

S10 Distribution of twin plane spacing

Figure S2 presents typical twin plane spacing distributions found for each of the colloid treatments. Measured from TEM images of individual nanowires, the distribution and central tendency is seen more clearly for the smaller diameter nanowires as these structures had a greater number of twin planes per wire and therefore larger samples size. Examining each x-axis, it is apparent that the distribution width is an increasing function of nanowire diameter. This may be

expected from the work of Algra *et al.*[1] who found the following expression for the expected width of segment length distributions δN_s.

$$\delta N_s = \frac{4H_c(D)/h}{\Delta} \quad \text{...(S5)}$$

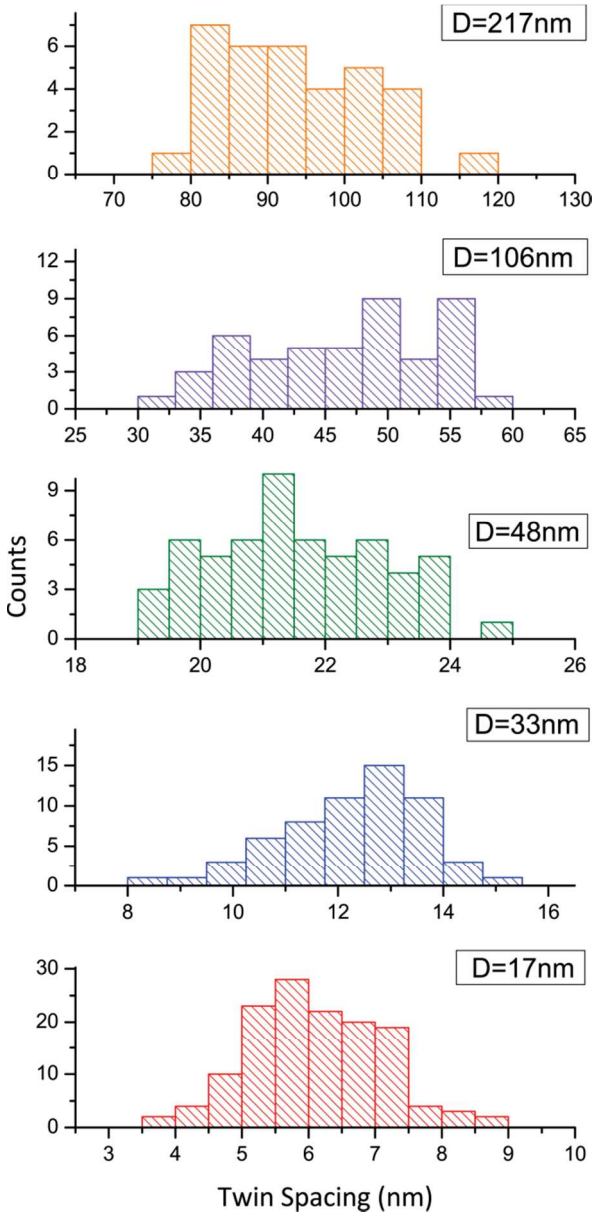

Figure S7 Histograms of twin plane spacing distribution as measured by TEM for representative nanowires from each of the colloid treatments.

References

1. Algra, R. E.; Verheijen, M. A.; Feiner, L.-F.; Immink, G. G. W.; Enckevort, W. J. P. v.; Vlieg, E.; Bakkers, E. P. A. M. The Role of Surface Energies and Chemical Potential During Nanowire Growth. *Nano Lett.* **2011**, 11, 1259–1264.

2. Algra, R. E.; Verheijen, M. A.; Borgstrom, M. T.; Feiner, L. F.; Immink, G.; van Enckevort, W. J. P.; Vlieg, E.; Bakkers, E. Twinning Superlattices in Indium Phosphide Nanowires. *Nature* **2008**, 456, 369-372.

3. Wallentin, J.; Ek, M.; Wallenberg, L. R.; Samuelson, L.; Deppert, K.; Borgstro□m, M. T. Changes in Contact Angle of Seed Particle Correlated with Increased Zincblende Formation in Doped InP Nanowires. *Nano Lett.* **2010**, 10, 4807–4812.